PCCP
Physical Chemistry Chemical Physics

Accepted Manuscript

This article can be cited before page numbers have been issued, to do this please use: S. Liu, X. Du, K. Ji, L. Lv and Y. Zhou, *Phys. Chem. Chem. Phys.*, 2025, DOI: 10.1039/D5CP01219H.

ROYAL SOCIETY OF CHEMISTRY

rsc.li/pccp

View Article Online
DOI: 10.1039/D5CP01219H

Mechanism of azeotrope elimination in the ethyl propionate–ethanol system using ionic liquid HMIMOAc as an entrainer: Experimental and theoretical insights

Shuyan Liu, Xiuyu Du, Kuan Ji, Lili Lv, Yu Zhou*

Shandong Sino-Japanese Center for Collaborative Research of Carbon Nanomaterials, College of Chemistry and Chemical Engineering, Qingdao University, Qingdao 266071, China.

A submission to: *Physical Chemistry Chemical Physics*

***To whom correspondence should be addressed.**

Dr. Yu Zhou

Email: zhouyu@qdu.edu.cn

View Article Online
DOI: 10.1039/D5CP01219H

Abstract

Ionic liquids (ILs) are highly effective entrainers for extractive distillation of azeotropes, owing to their unique physicochemical properties. However, the intrinsic molecular mechanisms underlying the role of ILs in azeotropic separation process remain insufficiently understood. To investigate the intrinsic causes of the azeotropy elimination by ILs, the study focused on the *ν*(O−D) region of the ethanol employing both experimental and theoretical methods to investigate the microstructural properties of the ethyl propionate (EP)−ethanol azeotrope before and after separation by the 1-hexyl-3-methylimidazole acetate (HMIMOAc). The key findings are as follows: (1) The interaction between HMIMOAc and ethanol is significantly stronger than that between EP and ethanol. (2) The interaction between $[OAc]^-$ in HMIMOAc and ethanol plays a critical role in eliminating the azeotropy. (3) Ethanol self-aggregates, EP−ethanol interaction complexes, and HMIMOAc−ethanol interaction complexes, were identified and characterized using excess spectroscopy and quantum chemical calculations.

Keywords: ionic liquid, azeotropy, interaction mechanisms, excess spectroscopy

View Article Online
DOI: 10.1039/D5CP01219H

1. Introduction

Ethyl propionate (EP) is used in a wide variety of applications including food, flavours and pharmaceuticals [1–3]. As a solvent, it is employed in producing cellulose ethers and esters, as well as dissolving natural and synthetic resins [4]. Its synthesis primarily relies on the esterification of propionic acid with ethanol, catalyzed by concentrated sulfuric acid [5]. However, EP and ethanol form an azeotrope at atmospheric pressure, making their separation particularly challenging [6]. High purity EP cannot be obtained through conventional distillation [7]. Among available separation techniques, extractive distillation is the most commonly employed, with the choice of entrainer playing a crucial role in the process [8,9].

Some organic solvents used as entrainers are highly volatile, toxic, and difficult to recycle, which can result in environmental pollution or high energy consumption. Therefore, selecting a new, environmentally friendly solvent is essential [10]. Recently, ionic liquids (ILs) have been widely regarded as excellent entrainers for the separation of azeotropic mixtures by extractive distillation due to their high thermal stability, high solubility, high decomposition temperature and other advantages [11–17]. These properties make ILs particularly suitable for extractive distillation. Currently, ILs are widely employed in the extractive distillation of various azeotropes, including water−alcohol [18–21], ester−alcohol [22–24], alcohol−ketone [25,26], and acetonitrile−water/alcohol/ester systems [27–29].

Changes in the microscopic properties of a system determine changes in its macroscopic properties. Specifically, the ability of ILs to eliminate azeotropes depends

View Article Online
DOI: 10.1039/D5CP01219H

on the microstructures of the system. Therefore, understanding the microstructures and interactions between ILs and azeotrope is crucial. Currently, the microstructural properties of IL−cosolvent and IL−IL systems have been extensively investigated [30–35]. For example, Jiang et al. investigated hydrogen bonding interactions between allyl- and ester-functionalized ILs and DMSO using infrared spectroscopy, excess infrared spectroscopy, and quantum chemical calculations, identifying possible complexes [36–38]. Lepre et al. examined the microstructures of BMIMOAc and $BMIMC(CN)_3$ ionic liquid mixtures through a combination of experiments and molecular dynamics simulations, revealing that as the concentration of $[C(CN)_3]^-$ increases, it preferentially occupies the upper and lower regions of the imidazolium ring, while $[OAc]^-$ tends to localize near the C2−H of the imidazolium ring [39]. However, these studies are limited to binary systems and do not fully reveal the mechanism of eliminating azeotropes. Recently, several research groups have begun to explore the molecular-level mechanism of ILs as entrainers. For instance, Chen et al. performed molecular simulations on the acetone−methanol−MMIMDMP system, finding that strong interactions between $[DMP]^-$ and methanol are crucial for eliminating the azeotropic behavior [40]. Despite these advances, studies on the structural properties of ternary mixtures containing ILs and azeotropes remain limited. Further exploration of the microstructural properties of IL-azeotrope systems is needed to uncover the molecular−level mechanisms behind azeotrope elimination.

The experimental results demonstrate that 1-hexyl-3-methylimidazole acetate (HMIMOAc) can eliminate the azeotrope of EP and ethanol when x(HMIMOAc) >

View Article Online
DOI: 10.1039/D5CP01219H

0.056, enabling effective separation of EP and ethanol [41]. In this study, HMIMOAc, EP, and ethanol were selected to investigate the microstructure characteristics of the IL−azeotrope ternary system. The microstructures were analyzed in detail by Fourier transform infrared spectroscopy (FTIR) and excess spectroscopy. The radial distribution function (RDF), mean square displacement (MSD), and spatial distribution function (SDF) of the system with different EP/ethanol component ratios in the presence or absence of ILs were investigated by molecular dynamics (MD) simulations, revealing the molecular-level mechanism behind the disruption of the EP−ethanol azeotrope by HMIMOAc. In addition, quantum chemical calculations were employed to identify the species of the mixtures and further validate the experimental results of infrared spectroscopy. Understanding and revealing the microstructures can help to select suitable ILs as entrainers for distillation, thereby enhancing separation efficiency.

2. Experimental section

2.1 Material and sample preparation

To avoid overlap between the region of ν(O−H) in ethanol and the region of ν(imidazolium C−H) in $[HMIM]^+$, ethanol was substituted by ethanol-d_6. Table 1 provides detailed information of ethanol-d_6, EP, and HMIMOAc. The binary mixtures (EP−ethanol-d_6 and HMIMOAc−ethanol-d_6) and ternary mixtures (EP−ethanol-d_6−HMIMOAc) were obtained by weighing. The concentrations of HMIMOAc in ternary system were 0.02 and 0.2, respectively.

View Article Online
DOI: 10.1039/D5CP01219H

Table 1 Detailed information of chemicals used.

Sample	Purity	Company
ethanol-d_6	99 %	Cambridge Isotopes Laboratories
EP	99 %	Shanghai Aladdin Biochemical Technology Co., Ltd.
HMIMOAc	98 %	Shanghai Cheng Jie Chemical Co., Ltd.

2.2 FTIR and excess spectroscopy

FTIR spectra were collected using a Nicolet Is50 FTIR spectrometer, equipped with a horizontally attenuated total reflection (ATR) cells at a 45° angle of incidence and 12 reflections, with ZnSe crystals, and an MCT detector to obtain the vibrational regions of ν(O−D). Excess spectroscopy was employed to enhance the apparent resolution and provide more detailed information on molecular interactions and solution structures. More details have been provided in previous studies [42,43].

2.3 Quantum chemical calculations

Optimization of vibrational geometries, energies, and vibrational frequencies of complexes was conducted using the M06-2X method [44] and the 6-311++G** basis set [45–47] in Gaussian 16 software [48–50]. Initially, the geometry of the monomers was first optimized. Then, the initial structure of each interacting complex was obtained by placing one of the monomers around all possible interaction sites of the other monomers. To enhance accuracy, the energy was corrected using the basis set superposition error (BSSE) and the frequency was corrected using the frequency correction factor (0.947) [51,52]. The most widely used correction method is Boys and Bernardi's Counterpoise

View Article Online
DOI: 10.1039/D5CP01219H

Procedure (CP) [52].

2.4 MD simulations

The binary systems of EP (1)−ethanol (2) and the pseudo-binary systems of EP (1)−ethanol (2)−HMIMOAc (3) were simulated. In the pseudo-binary systems, the mole fractions of the components were the same as in the binary system, defined as follows:

$$x_1^{'} = \frac{n_1}{n_1 + n_2}$$

$$x_2^{'} = \frac{n_2}{n_1 + n_2}$$

$$x_3 = \frac{n_3}{n_1 + n_2}$$

where n_1, n_2, and n_3 represent the number of molecules of EP, ethanol, and HMIMOAc ion pairs, respectively. The total number of molecules in the binary system was set to 1000. For the pseudo-binary systems containing the IL, 56 pairs of ion pairs were added to achieve a molar ratio x_3 of 0.056, consistent with the minimum addition of IL in the experiment. The pseudo-binary systems here are also often referred to as the ternary systems.

In this study, GAFF force field parameters were used to simulate both binary systems and the ternary systems, with topology files are generated by sobtop software [53]. The error between the simulated density and the experimental density is less than 3 % (Table 2), which proves that the system is suitable for the field and the simulation reliability is high. The initial structure was constructed using Packmol software with periodic boundary conditions in x, y, and z directions [54]. The truncation distance for non-bonding interactions was set to 1.0 nm and the long-range Coulomb interactions

View Article Online
DOI: 10.1039/D5CP01219H

were corrected using the Particle Mesh Ewald (PME) method.

Table 2 Comparison of simulated and experimental densities (g/cm^3) of pure EP, ethanol, and HMIMOAc at 298.15 K.

Pure chemical	Simulation	Experiment	Errors
EP	0.89	0.89	0.0 %
ethanol	0.77	0.79	−2.5 %
HMIMOAc	1.01	1.02	−1.0 %

The system underwent energy minimization before MD simulations were initiated. A 10 ns simulation was conducted to allow the system to reach equilibrium, followed by an additional 20 ns of MD simulations, from which data were collected for analysis and interpretation. The NPT system was set to 298.15 K, 1.0 atm. All MD simulations were performed using GROMACS 2022.3 software package [55]. SDFs were calculated using the TRAVIS package and viewed using the VMD program [56].

3. Results and discussions

3.1 Analysis of *ν*(O−D) region

3.1.1 FTIR and excess spectral analyses of binary systems

The microstructures of the HMIMOAc−azeotrope ternary system are highly complex, potentially involving various molecular forms and interaction complexes. This complexity makes it challenging to directly obtain information about the microstructures solely through infrared and excess spectroscopy of the HMIMOAc−azeotrope ternary system alone. To address this, it is necessary to examine the structural properties of the corresponding binary systems in great detail.

We initially analyzed the spectral characteristics of the EP−ethanol-d_6 and

View Article Online
DOI: 10.1039/D5CP01219H

HMIMOAc−ethanol-d_6 binary systems in the ν(O−D) region in Fig. 1. In the EP−ethanol-d_6 system (Fig. 1A), the intensity of ν(O−D) decreases monotonically as the concentration of ethanol-d_6 gradually decreases. The peak at 2467.6 cm^{-1} in the infrared spectra of pure ethanol-d_6 was observed to gradually blue shift to higher wavenumbers with adding EP. In contrast, in the HMIMOAc−ethanol-d_6 system (Fig. 1B), the intensity of ν(O−D) gradually decreased and underwent a red shift to lower wavenumbers. According to the literature [57], the hydrogen bonds associated with ν(O−D) are redshift hydrogen bonds. Thus, the blue shift observed in the EP−ethanol-d_6 system indicates a weakening of the hydrogen bonds involving ν(O−D), whereas the red shift observed in the HMIMOAc−ethanol-d_6 system suggests a strengthening of these hydrogen bonds. These results suggest that IL exhibits stronger hydrogen bonding interactions with ethanol compared to EP.

View Article Online
DOI: 10.1039/D5CP01219H

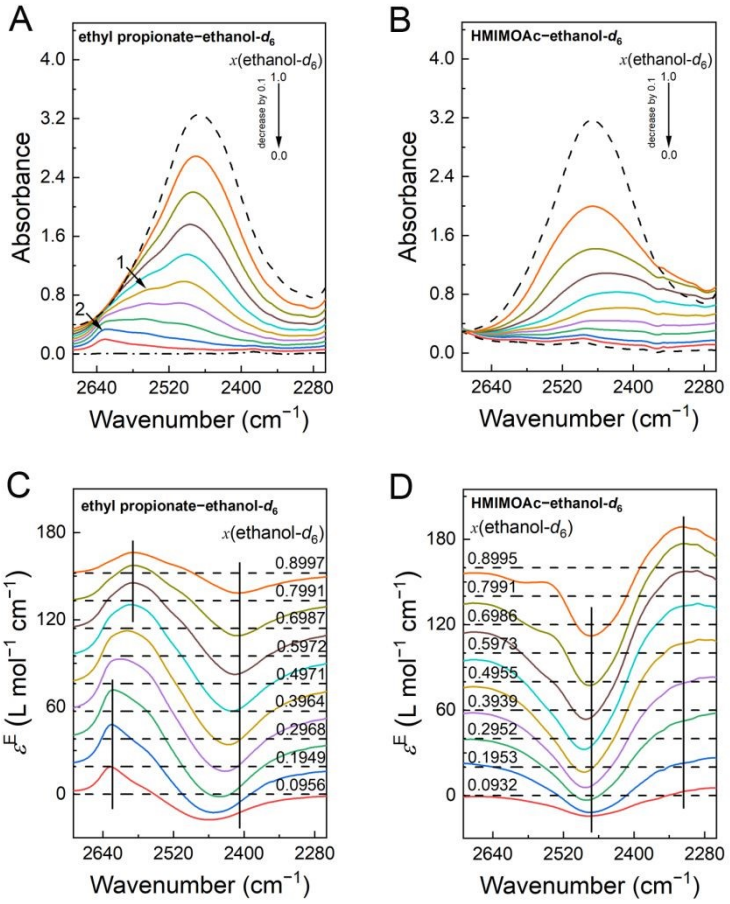

Fig. 1 FTIR spectra (A, B) and excess infrared spectra (C, D) of the EP−ethanol-d_6 and HMIMOAc−ethanol-d_6 systems in the ν(O−D) region.

The excess spectra of the binary systems EP−ethanol-d_6 and HMIMOAc−ethanol-d_6 are depicted in Fig. 1C and 1D, respectively. Each excess spectrum exhibits distinct peaks, indicating variations in species and interactions within the mixture. In both binary systems, a negative broad band can be observed in the range of 2500−2400 cm^{-1}. This broad band consists of multiple peaks, reflecting changes involving multiple complexes in this region. According to the literature, the absorption in this wavenumber range is mainly from larger alcohol aggregates such as cyclic tetramers, pentamers and other larger structures [58–60]. The negative excess peaks in this region indicate a decrease in larger alcohol aggregates in EP−ethanol-d_6 and HMIMOAc−ethanol-d_6 mixtures

View Article Online
DOI: 10.1039/D5CP01219H

compared to pure ethanol-d_6. Larger aggregates correspond to ν(O−D) peaks at lower wavenumbers, while their blue shift to higher wavenumbers suggests a transition from larger to smaller aggregates.

Significant positive excess peaks were also observed in the excess spectra of the binary systems. In the EP−ethanol-d_6 system, a broad positive excess band was observed at higher wavenumber than the negative excess peak (Fig. 1C). Conversely, in the HMIMOAc−ethanol-d_6 system, the positive excess peak appeared at a lower wavenumber (Fig. 1D). In the EP−ethanol-d_6 system, the positive excess band consisted of two distinct peaks at 2625.7 cm^{-1} and 2588.5 cm^{-1}, respectively. According to the literature [59,61], the excess peaks at 2588.5 cm^{-1} were associated with ethanol cyclic trimers, suggesting an increase in trimer content in the mixtures compared to pure ethanol-d_6. The relative abundance of these trimers decreased as the ethanol-d_6 concentration decreases. The intensity of the positive excess peak at 2625.7 cm^{-1} gradually increased with the increase in EP content, likely corresponding to interaction complex between ethanol-d_6 and EP. The formation of this interaction complex is responsible for the azeotropic behavior of the system.

In the HMIMOAc−ethanol-d_6 system, positive excess peaks were observed at 2317.1 and 2543.2 cm^{-1}. Notably, the latter peak appeared only at x'(ethanol-d_6) = 0.9 and 0.8, which may be cyclic trimer of ethanol. However, its content decreased with the decreasing ethanol concentration. The wavenumber of the trimer peak in HMIMOAc−ethanol-d_6 system was slightly lower than that in the EP−ethanol-d_6 system. These results indicate that the IL exerts a more pronounced effect on ethanol-

View Article Online
DOI: 10.1039/D5CP01219H

d_6 compared to EP.

3.1.2 FTIR and excess spectral analyses of ternary systems

According to the literature, the minimum IL concentration required to break azeotrope is 0.056 [41]. In this study, the mole fractions of IL in the EP−ethanol-d_6−HMIMOAc ternary system were set at 0.02 and 0.2 to observe the microstructural changes before and after breaking azeotrope. The FTIR and excess spectra of ν(O−D) region for the two ternary systems are shown in Fig. 2. The FTIR spectral features of these two ternary systems exhibit significant differences. When x(IL) = 0.02 (Figs. 2A and 2C), the spectral features were similar to those in the EP−ethanol-d_6 system (Figs. 1A and 1C). The ν(O−D) observed in pure ethanol-d_6 was gradually shifted to higher wavenumbers accompanied by the emergence of two shoulder peaks at higher wavenumbers. Conversely, when x(IL) = 0.2 (Figs. 2B and 2D), the spectral characteristics were similar to those of the HMIMOAc−ethanol-d_6 system (Figs. 1B and 1D).

View Article Online
DOI: 10.1039/D5CP01219H

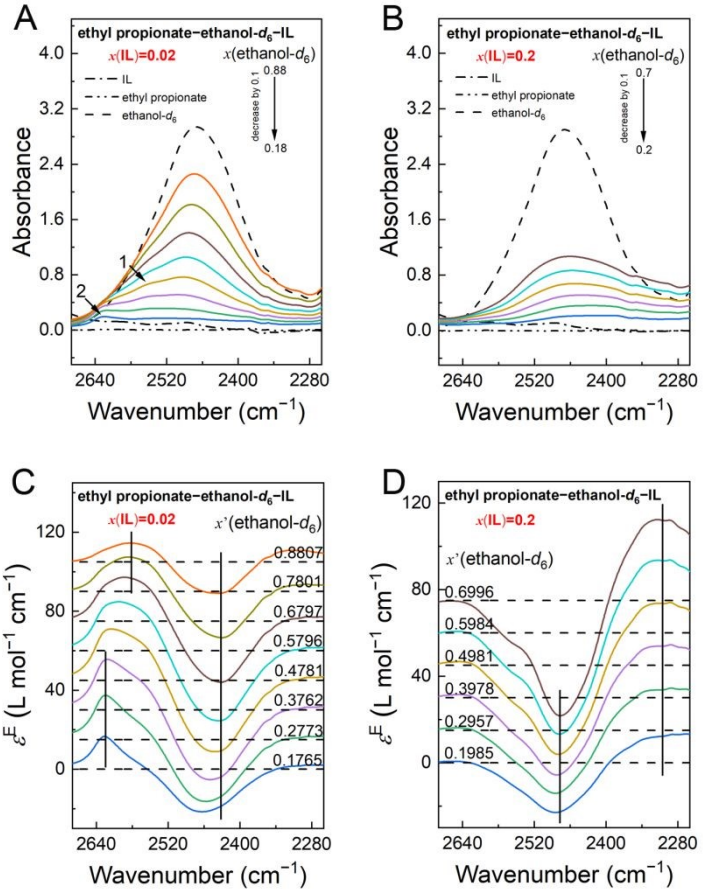

Fig. 2 FTIR spectra (A, B) and excess infrared spectra (C, D) of the EP−ethanol-d_6−HMIMOAc systems in the ν(O−D) region.

In excess spectra of both EP−ethanol-d_6−HMIMOAc ternary systems, a broader negative spectral band was observed in the range of 2500−2400 cm^{-1}, consistent with the binary systems. This negative band may be associated with the reduction of larger ethanol aggregates within the mixture. When x(IL) = 0.02 (Fig. 2C), broad positive bands appeared at approximately 2580.3 and 2625.7 cm^{-1} were observed, consistent with the EP−ethanol-d_6 binary system. The two peaks may be associated with the ethanol cyclic trimer and EP−ethanol-d_6 interacting complexes. When x(IL) = 0.2, the excess spectra displayed a positive excess peak at 2537.9 and 2303.1 cm^{-1}, which may be associated with the ethanol cyclic trimer, and the ethanol-d_6−HMIMOAc interacting

View Article Online
DOI: 10.1039/D5CP01219H

complexes, respectively. Notably, the excess peak, associated with the EP−ethanol-d_6 interaction complex, was absent, suggesting that the HMIMOAc disrupted the EP−ethanol azeotropic interaction.

To validate these spectral assignments and understand the structural changes, quantum chemical calculations were performed. The structures of ethanol trimers, tetramers, and pentamers were optimized, along with the most stable configurations and corresponding vibrational frequencies for the EP–ethanol polymer and various complexes, including, 2[HMIM]$^+$[OAc]$^-$−ethanol/EP, [HMIM]$^+$[OAc]$^-$−ethanol/EP, [HMIM]$^+$/[OAc]$^-$−ethanol/EP. Table 3 summarizes the optimal ν(O−H) frequencies for ethanol in different complexes. Although the calculated and observed frequencies are not identical, a linear correlation was identified as shown in Fig. 3 [62,63], demonstrating strong agreement between the experimental and calculated results, indicating that the assignment is reasonable. In the EP−ethanol-d_6 system, the positive excess peak at about 2625.7 cm^{-1} can be assigned to the EP−ethanol-d_6 interaction complex. This peak persists in the EP−ethanol-d_6−HMIMOAc system with x(IL) = 0.02, indicating that azeotrope has not been fully disrupted. In the HMIMOAc−ethanol-d_6 and EP−ethanol-d_6−HMIMOAc (x(IL) = 0.2) systems, the positive excess peak at 2303.1 cm^{-1} is confirmed to originate from the interaction between HMIMOAc and ethanol.

View Article Online
DOI: 10.1039/D5CP01219H

Table 3 The calculated ν(O−H) in EP−ethanol−HMIMOAc system.

Complex	ν(O−H)/cm^{-1}
ethanol	3707.6
[HMIM]$^+$-ethanol	3690.7
EP-ethanol	3664.7
ethanol-ethanol	3645.5
Cyclic trimer of ethanol	3586.4
Cyclic tetramer of ethanol	3546.9
Cyclic pentamer of ethanol	3484.3
[HMIM]$^+$[OAc]$^-$−ethanol	3213.7
[OAc]$^-$−ethanol	3095.8
2[HMIM]$^+$[OAc]$^-$−ethanol	3025.9

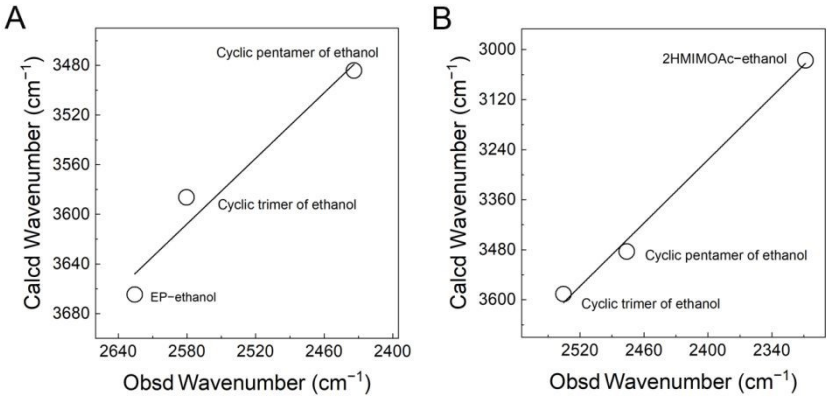

Fig. 3 The relationship between the calculated and observed wavenumbers of the ν(O−H) and ν(O−D) in EP−ethanol-d_6−HMIMOAc systems, respectively. x(IL) = 0.02 (A) and x(IL) = 0.2 (B).

3.2 Quantum chemical calculations analysis

Fig. 4 illustrates the optimized geometries of various interaction complexes, including EP−ethanol, ion pair−ethanol, ion cluster−ethanol, anion−ethanol, anion−EP, cation−ethanol, and cation−EP. In this study, the presence of hydrogen bond is identified based on the sum of van der Waals radii of O and H atoms (2.5 Å) [64]. Hydrogen bonds are depicted as dashed lines, with their distances and interaction

View Article Online
DOI: 10.1039/D5CP01219H

energies clearly labelled in the figure. To enhance the visualization of hydrogen bonds, the ion cluster−ethanol complexes are represented in stick form, with atoms forming hydrogen bonds shown in ball and stick mode.

The results confirm the existence of hydrogen bonds between EP/HMIMOAc and ethanol. In the ion cluster−ethanol interaction complexes, both the H and O atoms on the ethanol hydroxyl group participate in hydrogen bonds with HMIMOAc. Similarly, in anion/cation−ethanol interaction complexes, the O−H group of ethanol forms hydrogen bonds, identifying it as the main interaction site of ethanol.

A comparison of the absolute values of interaction energies shown in Fig. 4A, 4B, and 4C reveals that the absolute value of interaction energy between HMIMOAc and ethanol is significantly larger than that between EP and ethanol. This stronger interaction allows the HMIMOAc to disrupt the EP−ethanol interaction complex. Furthermore, a comparison of the hydrogen bonding distances in Fig. 4D and 4E shows that the anion−ethanol hydrogen bond has the shortest distance, indicating that the anion in the HMIMOAc forms the strongest hydrogen bond with ethanol. This strong interaction is the primary factor responsible for the elimination of azeotropy in the system.

View Article Online
DOI: 10.1039/D5CP01219H

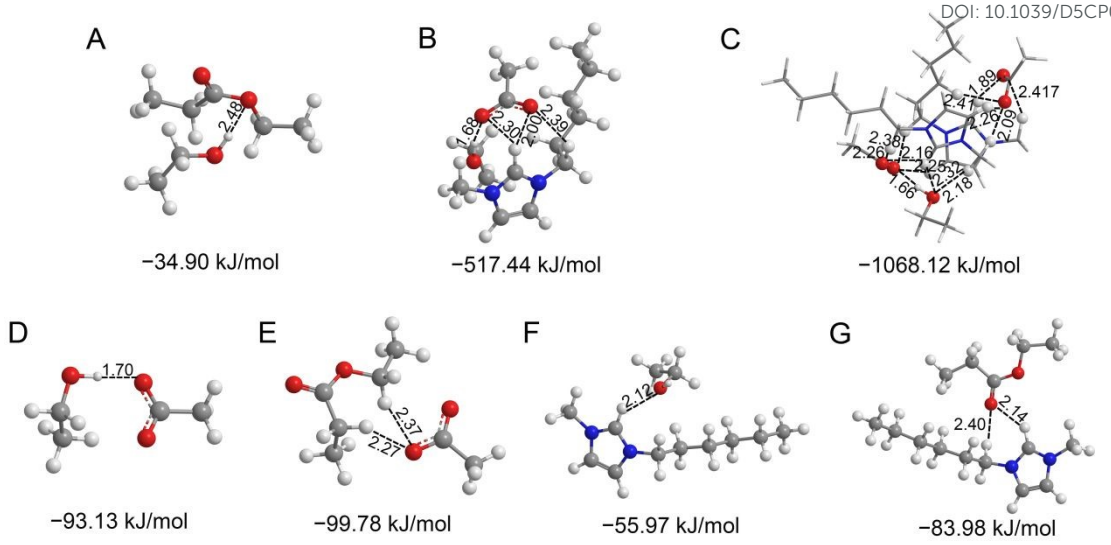

Fig. 4 Optimized geometries of EP−ethanol (A), $[HMIM]^+$-$[OAc]^-$−ethanol (B), 2$[HMIM]^+[OAc]^-$−ethanol (C), $[OAc]^-$−ethanol (D), $[OAc]^-$−EP (E), $[HMIM]^+$−ethanol (F), and $[HMIM]^+$−EP (G) complexes.

3.3 MD simulations analysis

As discussed in the previous section, the strong interaction between ethanol and anions is the main reason for the elimination of EP−ethanol azeotropy. To further explore the structural properties of the mixtures in binary and ternary systems, detailed molecular-scale information was thoroughly investigated by RDF, SDF, and MSD.

The RDF describes the variation in the density of target atoms within a distance r from the reference atom, relative to the average density of the target atoms. As discussed in the quantum chemical calculations, the HMIMOAc exhibits stronger interactions with ethanol. Therefore, the analysis primarily focuses on the RDF associated with ethanol. The RDFs of ethanol (O)−ethanol (O) and ethanol (O)−EP (O) with and without HMIMOAc conditions are depicted in Fig. 5. In the figure, x_1 is the mole fraction of EP in the ethanol−EP system and x_1' is the mole fraction of EP in the

View Article Online
DOI: 10.1039/D5CP01219H

ethanol−EP−IL system. As illustrated, the first peaks in the two systems are located near 0.27 nm. It is noteworthy that when ethanol and EP molecules interact with ethanol, they occupy similar spatial positions in the same distance layer. However, by comparing the peak heights of the first peaks in Figs. 5A and 5B, it can be seen that the first peak of ethanol−EP is lower than that of ethanol−ethanol, indicating a stronger hydrogen bonding interaction between ethanol molecules than that between ethanol and EP.

Additionally, the peaks of both RDFs decrease significantly upon the addition of HMIMOAc, especially in the EP-rich mixtures. For example, in the x(EP)/x'(EP) = 0.8 system (Fig. 5A), the first peak of the ethanol−ethanol decreased from 11.7 to 2.7 after the addition of HMIMOAc, indicating a significant structural change around the ethanol molecule, induced by the strong ethanol−$[OAc]^-$ interaction. Interestingly, the RDF of ethanol−ethanol in the system with x'(EP) = 0.8 shows a broad distribution, with a peak greater than 1 in the range of r = 0.4 ~ 1 nm, indicating the formation of large ethanol clusters. This is consistent with the experimental stratification at this concentration. In contrast, the RDFs of ethanol−EP display peaks lower than 1 within 1 nm, suggesting that EP molecules are difficult to approach ethanol molecules in the IL-containing system.

View Article Online
DOI: 10.1039/D5CP01219H

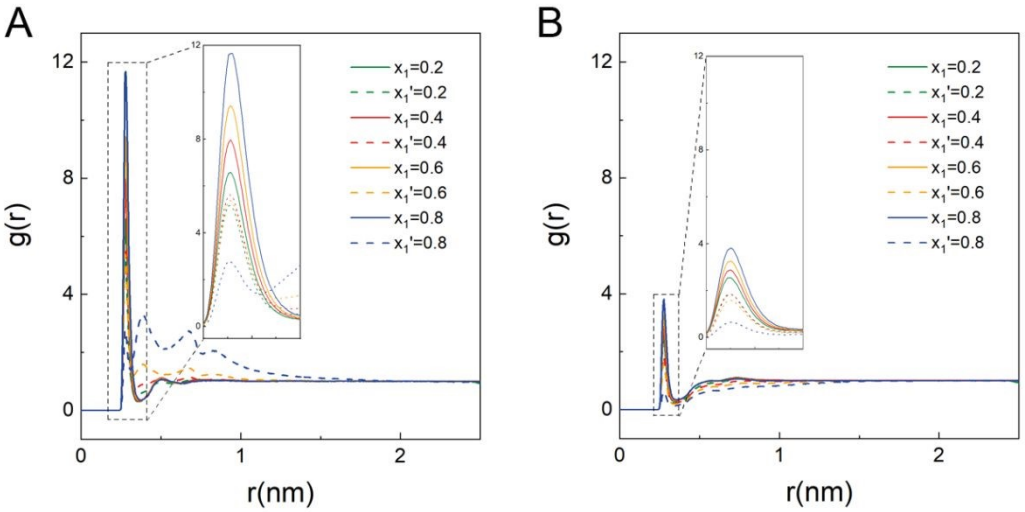

Fig. 5 RDFs of ethanol (O)−ethanol (O) (A) and ethanol (O)−EP (O) (B). The solid lines represent the systems without IL, and the dashed lines represent the systems with IL.

The RDFs also reflect the relative strength of interactions between two species in the system. The addition of HMIMOAc leads to a reduction in the RDF peaks for both ethanol−ethanol and ethanol−EP, suggesting that interactions involving ethanol−ethanol and ethanol−EP are weakened, while other interactions in the system are enhanced. The RDFs of ethanol−$[HMIM]^+$/$[OAc]^-$ in the system are depicted in Fig. 6. As can be seen from the figure, the peak value for ethanol−$[OAc]^-$ is much higher than that of the others, indicating it is the strongest interaction in the mixtures. This strong interaction is primarily responsible for the disruption of azeotrope at the molecular level. Furthermore, the role of anions becomes more important in EP-rich mixtures. The RDF peak for ethanol−$[OAc]^-$ is twice that of ethanol−ethanol at *x*'(EP) = 0.2 and reaches 30 times that of ethanol−ethanol at *x*'(EP) = 0.8, with most of the ethanol molecules being 'trapped' by $[OAc]^-$ anion.

View Article Online
DOI: 10.1039/D5CP01219H

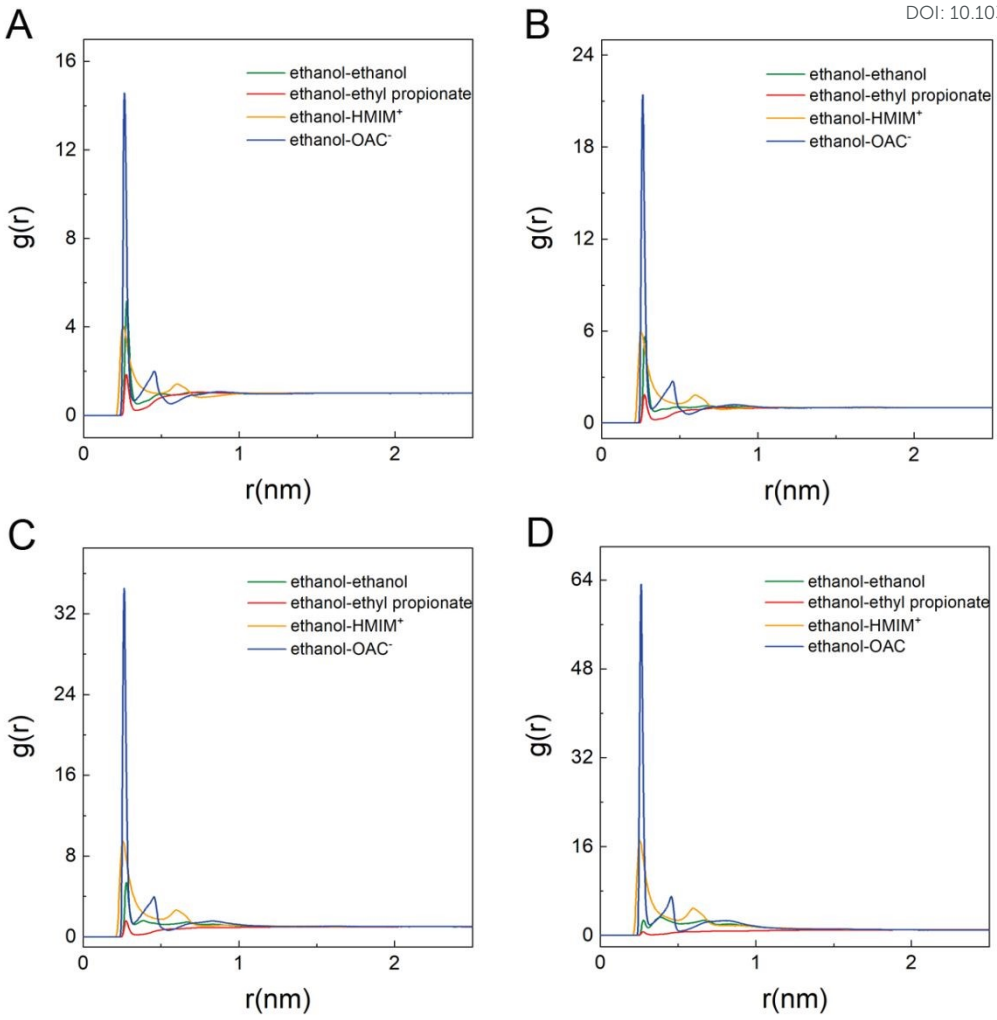

Fig. 6 RDFs of ethanol−ethanol, ethanol−EP, ethanol−$[HMIM]^+$, and ethanol−$[OAc]^-$ in systems with the IL at *x*'(EP) = 0.2(A), 0.4(B), 0.6(C), and 0.8(D), respectively.

The dynamic properties of EP, ethanol, $[HMIM]^+$, and $[OAc]^-$ can be studied directly by MSD. Since infinite time simulations are not feasible in practice, self-diffusion coefficients are determined from finite-time simulations by calculating the slopes of the MSD curves (Fig. 7) in the range where the curves are relatively flat and exhibit small statistical errors. The calculation range selected in this study is 5000−15000 ps and the self-diffusion coefficients are shown in Table 4. Smaller value of MSD indicates the slower diffusion rate and the stronger interaction. In Table 4, it is

View Article Online
DOI: 10.1039/D5CP01219H

evident that the MSD values for $[OAc]^-$ and ethanol are consistently smaller, regardless of the concentration, indicating stronger interaction between these molecules. Furthermore, as shown in Fig. 7, that the minimal difference in the degree of deflection between $[OAc]^-$ and ethanol further supports the conclusion that there is a strong interaction between $[OAc]^-$ and ethanol.

Table 4 The self-diffusion coefficients of $[HMIM]^+$, $[OAc]^-$, EP, and ethanol obtained from MD simulations.

$x'_{(EP)}$	$D_{[HMIM]^+}$ $\times 10^{-6}$ cm^2/s	$D_{[OAc]^-}$ $\times 10^{-6}$ cm^2/s	$D_{[EP]}$ $\times 10^{-6}$ cm^2/s	$D_{[ethanol]}$ $\times 10^{-6}$ cm^2/s
0.2	1.871	1.467	7.242	5.838
0.4	1.597	1.414	7.190	5.373
0.6	1.458	1.360	8.083	5.000
0.8	0.907	0.840	9.058	2.356

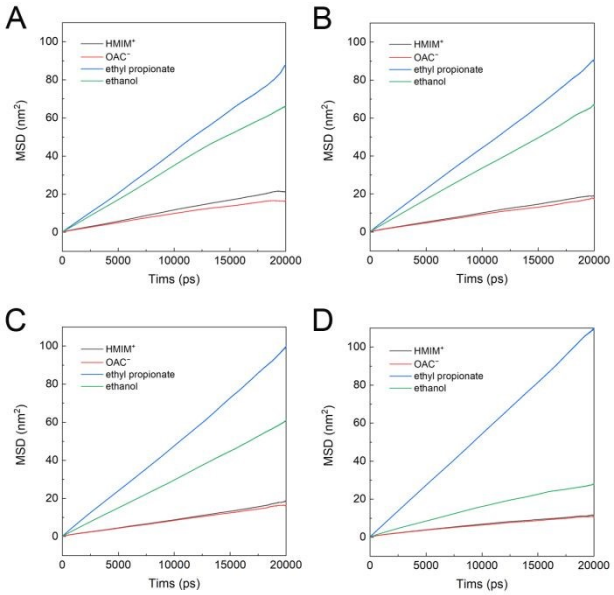

Fig. 7 MSD of different molecules in EP−ethanol−HMIMOAc ternary system at x'(EP) = 0.2(A), 0.4(B), 0.6(C), and 0.8(D), respectively.

To visualize the distribution around the ethanol molecule more intuitively, the SDF of $[OAc]^-$ in the presence of ethanol was calculated and is shown in Fig. 8A−D.

View Article Online
DOI: 10.1039/D5CP01219H

As the mole fraction of EP gradually increases, the average density of $[OAc]^-$ around ethanol also increases, indicating a stronger interaction between $[OAc]^-$ and ethanol. Notably, $[OAc]^-$ is primarily distributed near the −OH group of ethanol. Fig. 8E−H shows the SDFs of ethanol (red) and EP (yellow) around $[OAc]^-$. Two almost symmetrical cap regions are evident around the two O atoms of the anion. At higher concentrations of EP (x'(EP) = 0.6 and 0.8), the average density of ethanol around $[OAc]^-$ is significantly higher than that of EP. This suggests that ethanol molecules are repelled to $[OAc]^-$ by the extrusion of more and more EP in the system. Furthermore, ethanol is mainly distributed near the O atoms of $[OAc]^-$.

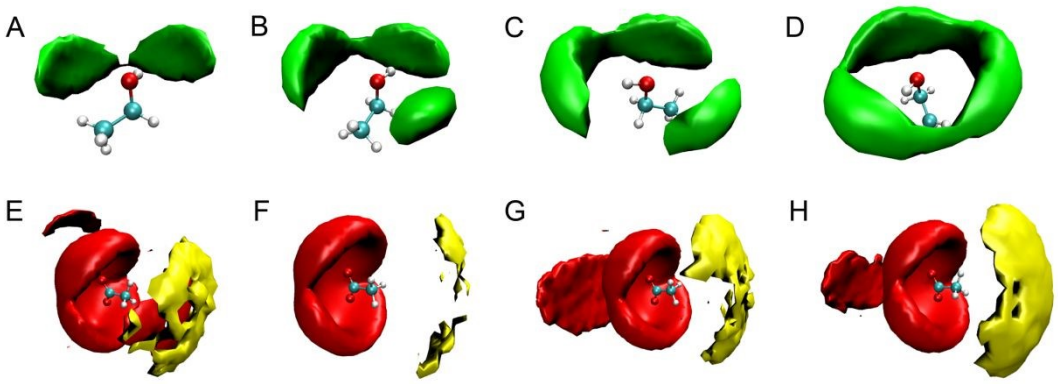

Fig. 8 SDFs of $[OAC]^-$ around ethanol in systems with the IL at x'(EP) = 0.2(A), 0.4(B), 0.6(C), 0.8(D), at same isovalue. SDFs of ethanol (red) and EP (yellow) around $[OAC]^-$ in systems with the IL at x'(EP) = 0.2(E), 0.4(F), 0.6(G), 0.8(H), at same isovalue.

4. Conclusions

This study systematically investigates the microstructural properties of the EP−ethanol−HMIMOAc system through a combination of experimental and theoretical approaches, providing insights into the molecular properties of HMIMOAc as an extractive distillation entrainer. A detailed vibrational analysis was carried out for the

View Article Online
DOI: 10.1039/D5CP01219H

ν(O−D) region of ethanol. The spectral characteristics of the ternary system of EP−ethanol−HMIMOAc before and after the elimination of azeotropy were investigated by spectral analysis. Several peaks associated with large size ethanol self-aggregates and EP/HMIMOAc−ethanol interaction complexes were identified. EP−ethanol interaction complexes were identified in the EP−ethanol-d_6 and EP−ethanol-d_6−IL (x(IL) = 0.02) systems, which contribute significantly to the formation of azeotrope in the EP−ethanol-d_6 system. In addition, HMIMOAc−ethanol-d_6 interaction complexes were identified in the HMIMOAc−ethanol-d_6 and EP−ethanol-d_6−IL (x(IL) = 0.2) systems. All methods consistently demonstrated that the interaction between HMIMOAc and ethanol is stronger than that between EP and ethanol, which revealed that the $[OAC]^-$ in the IL interacts more strongly with ethanol, providing a molecular-level explanation for the elimination of the azeotropy.

Based on these findings, the intrinsic molecular mechanisms for the elimination of the azeotropy were revealed: First, the interaction between HMIMOAc and ethanol is stronger than that between HMIMOAc and EP, thereby altering the relative volatility of the two components in the system. Second, the stronger interaction HMIMOAc and ethanol disrupts the EP−ethanol interaction complexes. At low HMIMOAc mole fractions (x(IL) < 0.056), the HMIMOAc concentration is insufficient to completely disrupt the EP−ethanol interaction complexes, allowing azeotropy to persist. However, when the IL mole fraction exceeds 0.056, HMIMOAc effectively disrupts all EP−ethanol interaction complexes, thereby completely eliminating the azeotropic behavior.

View Article Online
DOI: 10.1039/D5CP01219H

Author contributions

Shuyan Liu: Conceptualization, Methodology, Validation, Writing–original draft. Xiuyu Du: Formal analysis, Data management. Kuan Ji: Formal analysis. Lili Lv: Writing–review&editing. Yu Zhou: Supervision, Writing–review &editing, Funding acquisition.

Data availability

The data supporting the findings of this study are available within the article.

Conflicts of interest

There are no conflicts to declare.

Acknowledgments

This work was supported by the National Natural Science Foundation of China (Grant No. 22073054 and No. 52203119) and the Natural Science Foundation of Shandong Province (Project No. ZR2024QB052). We thank Dr. Xiyue Cao (Instrumental Analysis Center, Qingdao University) for help.

References

1 S. S. Kanwar, H. K. Verma, R. K. Kaushal, R. Gupta, S. S. Chimni, Y. Kumar and G. S. Chauhan, Effect of Solvents and Kinetic Parameters on Synthesis of Ethyl Propionate Catalysed by Poly (AAc-co-HPMA-cl-MBAm)-Matrix-Immobilized Lipase of Pseudomonas aeruginosa BTS-2., *World J Microbiol Biotechnol*, 2005, **21**, 1037–1044.

2 Z. Xing, Y. Gao, H. Ding, X. Wang, L. Li and H. Zhou, Isobaric vapor–liquid

equilibrium for ternary system of ethanol, ethyl propionate and para-xylene at 101.3 kPa, *Chinese Journal of Chemical Engineering*, 2018, **26**, 560–565.

3 R. Cheramangalath Balan and B. Rajakumar, Photo Oxidation Reaction Kinetics of Ethyl Propionate with Cl Atom and Formation of Propionic Acid, *J. Phys. Chem. A*, 2018, **122**, 8274–8285.

4 S. Li, X. Huang, Q. Huang, T. Guo, S. Yun, C. Ban and G. Shen, Vapor-liquid equilibrium in the binary and ternary systems containing ethyl propionate, ethanol and alkane at 101.3 kPa, *Fluid Phase Equilibria*.

5 E. M. Faber and E. E. Reid, STUDIES IN ESTERIFICATION. IX. THE ESTERIFICATION OF ACETIC AND PROPIONIC ACIDS BY METHYL, ETHYL, PROPYL, ISOBUTYL AND ISOAMYL MERCAPTANS., *J. Am. Chem. Soc.*, 1917, **39**, 1930–1938.

6 Y. Song, Y. Du, R. Wang, H. Yan, F. Luo and L. Sun, Vapor–Liquid Equilibria and Conceptual Design of Extractive Distillation for Separating Ethanol and Ethyl Propionate, *J. Chem. Eng. Data*, 2020, **65**, 3428–3437.

7 T. Brouwer and B. Schuur, Bio-based solvents as entrainers for extractive distillation in aromatic/aliphatic and olefin/paraffin separation, *Green Chem.*, 2020, **22**, 5369–5375.

8 C. V. Manohar, T. Banerjee and K. Mohanty, Co-solvent effects for aromatic extraction with ionic liquids, *Journal of Molecular Liquids*, 2013, **180**, 145–153.

9 G. Li, S. Liu, G. Yu, C. Dai and Z. Lei, Extractive distillation using ionic liquids-based mixed solvents combined with dividing wall column, *Separation and Purification Technology*, 2021, **269**, 118713.

10 H. Cheng, K. Wang, Y. Wang, G. Zhao, Z. Zhu, J. Qi, L. Zhong, Y. Wang, H. Zhang and P. Cui, Mechanism Analysis and Multiobjective Optimization of Efficient and Energy-Saving Separation of Green Fuel Additives via Extractive Pressure Swing Distillation with an Ionic Liquid Mixed Entrainer, *Ind. Eng. Chem. Res.*, 2024, **63**, 5261–5275.

11 Z. Zhu, X. Geng, W. He, C. Chen, Y. Wang and J. Gao, Computer-Aided Screening of Ionic Liquids As Entrainers for Separating Methyl Acetate and Methanol via Extractive Distillation, *Ind. Eng. Chem. Res.*

12 Y. Deng, P. Besse-Hoggan, M. Sancelme, A.-M. Delort, P. Husson and M. F. Costa Gomes, Influence of oxygen functionalities on the environmental impact of imidazolium based ionic liquids, *J. Hazard. Mater.*, 2011, **198**, 165–174.

13 Z. Song, X. Li, H. Chao, F. Mo, T. Zhou, H. Cheng, L. Chen and Z. Qi, Computer-aided ionic liquid design for alkane/cycloalkane extractive distillation process, *Green Energy & Environment*, 2019, **4**, 154–165.

14 Y. Dong, Q. Yang, Z. Li and Z. Lei, Extractive distillation of the benzene and acetonitrile mixture using an ionic liquid as the entrainer, *Green Energy Environ.*, 2021, **6**, 444–451.

15 Y. Yang, H. Fan, T. Wu, G. Yang and B. Han, Complete degradation of high-loaded phenol using tungstate-based ionic liquids with long chain substituent at mild conditions, *Green Energy & Environment*, 2023, **8**, 452–458.

16 G. Zhang, B. Yang, S. Yang, Z. Lei and P. Xu, Heat-integrated extractive distillation

for separating tetrahydrofuran/methanol/water with ionic liquid-based mixed entrainer: Molecular mechanism and process integration, *Separation and Purification Technology*, 2025, **356**, 129843.

17 L. Zhou, M. Zhang, Y. Huo, L. Bai, S. He, J. Wang, C. Jia and X. Guo, Application of ionic liquids in single-molecule junctions: Recent advances and prospects, *Green Energy & Environment*, 2024, **9**, 1784–1801.

18 B. Diao, Z. Wang, H. Yang, L. Zhang, D. Xu, J. Gao and Y. Wang, Separation of azeotrope 2,2,3,3-tetrafluoro-1-propanol and water by extractive distillation using ionic liquids: Vapor-liquid equilibrium measurements and interaction analysis, *Journal of Molecular Liquids*, 2019, **292**, 111424.

19 V. K. P. Janakey Devi, P. S. T. Sai and A. R. Balakrishnan, Ammonium-Based Ionic Liquid as an Entrainer for the Separation of *n* -Propanol + Water and Isopropanol + Water Mixtures, *J. Chem. Eng. Data*, 2018, **63**, 498–507.

20 S. Liu, Z. Wang, R. Zhu, Z. Lei and J. Zhu, [EMIM][DCA] as an entrainer for the extractive distillation of methanol-ethanol-water system, *Green Energy & Environment*, 2021, **6**, 363–370.

21 P. Cui, Y. Wang, H. Cheng, Z. Wang, L. Xin, W. Xu, Y. Wang, G. Li and Z. Zhu, Efficient separating dipropyl ether/isopropanol/water azeotrope by extractive distillation with mixed entrainer based on ionic liquid, *Journal of Cleaner Production*, 2024, **479**, 143980.

22 J. M. Winnert, V. K. P. J. Devi and J. F. Brennecke, Using Dialkylimidazolium Ionic Liquids To Break the Methanol + Methyl Acetate Azeotrope, *Ind. Eng. Chem. Res.*, 2019, **58**, 22633–22639.

23 P. Wang, P. Yan, J. A. Reyes-Labarta, J. Gao, D. Xu, L. Zhang and Y. Wang, Liquid-liquid measurement and correlation for separation of azeotrope (dimethyl carbonate and ethanol) with different imidazolium-based ionic liquids, *Fluid Phase Equilibria*, 2019, **485**, 183–189.

24 H. Li, G. Sun, D. Li, L. Xi, P. Zhou, X. Li, J. Zhang and X. Gao, Molecular interaction mechanism in the separation of a binary azeotropic system by extractive distillation with ionic liquid, *Green Energy & Environment*, 2021, **6**, 329–338.

25 T. Wu, Q. Zhang, H. Xin, S. Li, T. Song and Z. Zhang, Study on the selective separation of methanol and methyl ethyl ketone from the azeotropic system using ionic liquids and their separation mechanism, *Journal of Molecular Liquids*, 2021, **343**, 117571.

26 W. Li, X. Fan, H. Guo, X. He, L. Wang and T. Zhang, Isobaric vapor-liquid equilibrium for 2-butanone + ethanol + acetate-based ionic liquids at 101.3 kPa, *Fluid Phase Equilibria*, 2022, **552**, 113298.

27 J. Zhu, H. Fan, B. Sun and H. Qi, Effect and Mechanism of 1-Hexyl-3-methylimidazolium-Based Ionic Liquids on the Isobaric Vapor–Liquid Equilibria of Methanol + Acetonitrile at 101.3 kPa, *J. Chem. Eng. Data*.

28 J. Zhu, Q. Li, M. Li, X. Song, H. Tang and Y. Liu, The isobaric vapor liquid equilibria of ethyl acetate + acetonitrile + bis(trifluoromethylsulfonyl)imide-based ionic liquids at 101.3 kPa, *Fluid Phase Equilibria*, 2016, **425**, 289–296.

29 T. Li, Q. Yang, H. Ding, J. Li, C. Peng and H. Liu, Amino Acid Based Ionic Liquids

as Additives for the Separation of an Acetonitrile and Water Azeotropic Mixture: COSMO-RS Prediction and Experimental Verification, *Ind. Eng. Chem. Res.*, 2015, **54**, 12143–12149.

30 L. Ma, M. Yang and K. Zhao, Interaction and microstructure in the binary mixture systems of ionic liquid and acetone by dielectric spectroscopy, *Journal of Molecular Liquids*, 2016, **220**, 295–303.

31 S. Zhou, G. Zhu, X. Kang, Q. Li, M. Sha, Z. Cui and X. Xu, Molecular dynamics simulation of the ionic liquid N-octylpyridinium tetrafluoroborate and acetonitrile: Thermodynamic and structural properties, *Chemical Physics Letters*, 2018, **701**, 1–6.

32 S. Gehrke, M. Von Domaros, R. Clark, O. Hollóczki, M. Brehm, T. Welton, A. Luzar and B. Kirchner, Structure and lifetimes in ionic liquids and their mixtures, *Faraday Discuss.*, 2018, **206**, 219–245.

33 I. V. Voroshylova, E. S. C. Ferreira, M. Malček, R. Costa, C. M. Pereira and M. N. D. S. Cordeiro, Influence of the anion on the properties of ionic liquid mixtures: a molecular dynamics study, *Phys. Chem. Chem. Phys.*, 2018, **20**, 14899–14918.

34 H. Chen, Z. Wang, P. Zhao, X. Xu, S. Gong, Z. Yu and Y. Zhou, Comparative study of the hydrogen bonding properties between bis(fluorosulfonyl)imide/bis(trifluoromethyl)sulfonylimide-based ether-functionalized ionic liquids and methanol, *Journal of Molecular Liquids*, 2021, **328**, 115333.

35 R. Zhao, X. Xu, Z. Wang, Y. Zheng, Y. Zhou and Z. Yu, Structural microheterogeneity and hydrogen bonding properties in the mixtures of two ionic liquids with a common imidazolium cation, *J. Mol. Liq.*, 2022, **368**, 120594.

36 Y. Jiang, X. Xu, M. Wang, Y. Zhou and Z. Wang, Comparative study of the hydrogen bonding interactions between ester-functionalized/non-functionalized imidazolium-based ionic liquids and DMSO, *Phys. Chem. Chem. Phys.*, 2023, **25**, 8789–8798.

37 Y. Jiang, X. Xu, S. Gong, X. Zhang, Y. Zhou and Z. Wang, Comparative study of the hydrogen bonding properties between allyl-functionalized/non-functionalized ionic liquids and DMSO, *Vibrational Spectroscopy*, 2022, **122**, 103412.

38 S. Liu, Y. Jiang, P. Zhao, X. Xu, X. Liu and Y. Zhou, Molecular behavior of 1-acetoxymethyl-3-methylimidazolium tetrafluoroborate and DMSO binary system, *Chemical Physics*, 2025, **588**, 112467.

39 L. F. Lepre, J. Szala-Bilnik, A. A. H. Padua, M. Traïkia, R. A. Ando and M. F. Costa Gomes, Tailoring the properties of acetate-based ionic liquids using the tricyanomethanide anion, *Phys. Chem. Chem. Phys.*, 2016, **18**, 23285–23295.

40 F. Chen, L. Zhang, Z. Liu and G. Yu, Cluster Formation and Its Role in the Elimination of Azeotrope of the Acetone–Methanol Mixture by Ionic Liquids, *Ind. Eng. Chem. Res.*, 2020, **59**, 13271–13282.

41 Z. Zhang, Z. Zhang, B. Dong, J. Chen, H. Xin and Q. Zhang, Vapor-liquid equilibrium experiment and model prediction for separating ethyl propionate and ethanol using ionic liquids with acetate anion, *Journal of Molecular Liquids*, 2020, **318**, 113688.

42 Q. Li, G. Wu and Z. Yu, The Role of Methyl Groups in the Formation of Hydrogen Bond in DMSO−Methanol Mixtures, *J. Am. Chem. Soc.*, 2006, **128**, 1438–1439.

43 Zhou Y., Xu J., Wang N.-N. and Yu Z.-W., Excess Spectroscopy: Concept and Applications, *Acta Phys. Chim. Sin.*, 2016, **32**, 239–248.

44 Y. Zhao and D. G. Truhlar, The M06 suite of density functionals for main group thermochemistry, thermochemical kinetics, noncovalent interactions, excited states, and transition elements: two new functionals and systematic testing of four M06-class functionals and 12 other functionals, *Theor Chem Account*, 2008, **120**, 215–241.

45 A. D. McLean and G. S. Chandler, Contracted Gaussian basis sets for molecular calculations. I. Second row atoms, Z=11–18 □.

46 R. Krishnan, J. S. Binkley, R. Seeger and J. A. Pople, Self-consistent molecular orbital methods. XX. A basis set for correlated wave functions □.

47 R. Krishnan, J. S. Binkley, R. Seeger and J. A. Pople, Self-consistent molecular orbital methods. XX. A basis set for correlated wave functions, *The Journal of Chemical Physics*, 1980, **72**, 650–654.

48 E. G. Hohenstein, S. T. Chill and C. D. Sherrill, Assessment of the Performance of the M05−2X and M06−2X Exchange-Correlation Functionals for Noncovalent Interactions in Biomolecules, *J. Chem. Theory Comput.*, 2008, **4**, 1996–2000.

49 M. J. Frisch, J. A. Pople and J. S. Binkley, Self-consistent molecular orbital methods 25. Supplementary functions for Gaussian basis sets, *The Journal of Chemical Physics*, 1984, **80**, 3265–3269.

50 M. J. Frisch, G. W. Trucks, H. B. Schlegel, G. E. Scuseria, M. A. Robb, J. R. Cheeseman, G. Scalmani, V. Barone, G. A. Petersson, H. Nakatsuji, X. Li, M. Caricato, A. V. Marenich, J. Bloino, B. G. Janesko, R. Gomperts, B. Mennucci, H. P. Hratchian, J. V. Ortiz, A. F. Izmaylov, J. L. Sonnenberg, D. Williams-Young, F. Ding, F. Lipparini, F. Egidi, J. Goings, B. Peng, A. Petrone, T. Henderson, D. Ranasinghe, V. G. Zakrzewski, J. Gao, N. Rega, G. Zheng, W. Liang, M. Hada, M. Ehara, K. Toyota, R. Fukuda, J. Hasegawa, M. Ishida, T. Nakajima, Y. Honda, O. Kitao, H. Nakai, T. Vreven, K. Throssell, J. A. Montgomery Jr., J. E. Peralta, F. Ogliaro, M. J. Bearpark, J. J. Heyd, E. N. Brothers, K. N. Kudin, V. N. Staroverov, T. A. Keith, R. Kobayashi, J. Normand, K. Raghavachari, A. P. Rendell, J. C. Burant, S. S. Iyengar, J. Tomasi, M. Cossi, J. M. Millam, M. Klene, C. Adamo, R. Cammi, J. W. Ochterski, R. L. Martin, K. Morokuma, O. Farkas, J. B. Foresman and D. J. Fox, 2016.

51 D. O. Kashinski, G. M. Chase, R. G. Nelson, O. E. Di Nallo, A. N. Scales, D. L. VanderLey and E. F. C. Byrd, Harmonic Vibrational Frequencies: Approximate Global Scaling Factors for TPSS, M06, and M11 Functional Families Using Several Common Basis Sets, *J. Phys. Chem. A*, 2017, **121**, 2265–2273.

52 S. F. Boys and F. Bernardi, The calculation of small molecular interactions by the differences of separate total energies. Some procedures with reduced errors, *Mol. Phys.*, 2002, **100**, 65–73.

53 Tian Lu, Sobtop, Version 1.0(dev3.1), http://sobereva.com/soft/Sobtop (accessed on August 9, 2022).

54 L. Martínez, R. Andrade, E. G. Birgin and J. M. Martínez, PACKMOL: A package for building initial configurations for molecular dynamics simulations, *J. Comput. Chem.*, 2009, **30**, 2157–2164.

55 P. Bauer, B. Hess, E. Lindahl, GROMACS 2022.3 Manual, 2022, **673**.

56 M. Brehm and B. Kirchner, TRAVIS - A Free Analyzer and Visualizer for Monte Carlo and Molecular Dynamics Trajectories, *J. Chem. Inf. Model.*, 2011, **51**, 2007–2023.

57 J. Joseph and E. D. Jemmis, Red-, Blue-, or No-Shift in Hydrogen Bonds: A Unified Explanation, *J. Am. Chem. Soc.*, 2007, **129**, 4620–4632.

58 U. Buck and F. Huisken, Infrared Spectroscopy of Size-Selected Water and Methanol Clusters, *Chem. Rev.*, 2000, **100**, 3863–3890.

59 R. W. Larsen, P. Zielke and M. A. Suhm, Hydrogen-bonded OH stretching modes of methanol clusters: A combined IR and Raman isotopomer study, *The Journal of Chemical Physics*, 2007, **126**, 194307.

60 Y.-Z. Zheng, Y. Zhou, G. Deng, R. Guo and D.-F. Chen, The structure and hydrogen-bond behaviours of binary systems containing ionic liquid 1-butyl-3-methylimidazolium tetrafluoroborate and methanol/ethanol, *Spectrochimica Acta Part A: Molecular and Biomolecular Spectroscopy*, 2019, **223**, 117312.

61 Y.-Z. Zheng, Y.-X. Jiang, Y. Zhou and Y.-C. Zhang, The molecular nature of the eliminating azeotropy of dimethyl carbonate–ethanol system by ionic liquid entrainer, *Separation and Purification Technology*, 2023, **305**, 122420.

62 Y. Zhou, Y.-Z. Zheng, H.-Y. Sun, G. Deng and Z.-W. Yu, Two-State or Non-Two-State? An Excess Spectroscopy-based Approach to Differentiate the Existing Forms of Molecules in Liquids Mixtures, *Sci. Rep.*, 2015, **5**, 16379.

63 H. He, H. Chen, Y. Zheng, X. Zhang, X. Yao, Z. Yu and S. Zhang, The Hydrogen-Bonding Interactions between 1-Ethyl-3-Methylimidazolium Lactate Ionic Liquid and Methanol, *Aust. J. Chem.*, 2013, **66**, 50.

64 P. Kalhor, Y. Zheng, H. Ashraf, B. Cao and Z. Yu, Influence of Hydration on the Structure and Interactions of Ethaline Deep-Eutectic Solvent: A Spectroscopic and Computational Study, *ChemPhysChem*, 2020, **21**, 995–1005.

View Article Online
DOI: 10.1039/D5CP01219H

Data availability

The authors confirm that the data supporting the findings of this study are available within the article.